telecom

MDPI

Article

OSNR-Aware Modeling and Optimization of Multi-Core Fiber-Based Spectrally–Spatially Flexible Optical Networks

Mirosław Klinkowski * and Marek Jaworski

National Institute of Telecommunications, 1 Szachowa Street, 04-894 Warsaw, Poland; m.jaworski@il-pib.pl
* Correspondence: m.klinkowski@il-pib.pl

Abstract: We focus on the optical signal-to-noise ratio (OSNR)-aware optical path (lightpath) planning problem in spectrally and spatially flexible optical networks (SS-FONs) connected using weakly coupled multi-core fibers (MCFs) in which distance-adaptive and super-channel transmission is realized using multiple modulation formats. In the SS-FON considered, the quality of transmission (QoT) of optical signals is degraded due to the inter-core crosstalk (XT) effect occurring in MCFs. To account for the XT impairment when planning lightpath connections, we make use of a reliable QoT model based on the OSNR estimation, in which the XT impairment is integrated with other physical-layer impairments. To model the lightpath planning optimization problem, we develop a novel mixed-integer programming (MIP) formulation that incorporates the OSNR model. In addition, we propose an efficient heuristic method that is capable of solving larger instances of the optimization problem considered. The results of numerical experiments indicate the low scalability of the MIP method due to the presence of XT and high effectiveness of the heuristic method. The analysis of three different network topologies and two types of MCFs shows a high impact of XT on network performance and limited performance gains from the presence of the central core in a 7-core MCF.

Keywords: space division multiplexing; elastic optical networks; multi-core fiber; inter-core crosstalk; routing; spatial mode and spectrum allocation; offline planning; network optimization; mixed integer programming; heuristics

check for updates

Citation: Klinkowski, M.; Jaworski, M. OSNR-Aware Modeling and Optimization of Multi-Core Fiber-Based Spectrally–Spatially Flexible Optical Networks. *Telecom* **2022**, *3*, 467–483. https://doi.org/10.3390/telecom3030025

Academic Editor: Bernard Cousin

Received: 20 June 2022
Accepted: 11 July 2022
Published: 13 July 2022

Publisher's Note: MDPI stays neutral with regard to jurisdictional claims in published maps and institutional affiliations.

Copyright: © 2022 by the authors. Licensee MDPI, Basel, Switzerland. This article is an open access article distributed under the terms and conditions of the Creative Commons Attribution (CC BY) license (https://creativecommons.org/licenses/by/4.0/).

1. Introduction

The evolution of communication networks is driven by the development and deployment of the 5th generation wireless networks (5G) [1]. The observed trends result in the increase in metro, cloud and data center traffic, broadband speed, and numbers of devices connected to the Internet. In this context, optical fiber networks are considered a key technology for building the underlying transport infrastructure capable of assuring high capacity, good scalability, low latency, carrier-class reliability, and adaptability to rapidly changing demand and traffic patterns for best resource utilization.

Spatially and spectrally flexible optical networks, which combine space division multiplexing (SDM) [2] with flexible-grid elastic optical network (EON) technologies [3], have been proposed as a long-term solution for ever-increasing capacity requirements in optical networks [4,5]. SDM allows for the parallel transmission of a number of spatial modes in suitable designed optical fibers, such as weakly coupled multi-core fibers [6]. Concurrently, EONs enable a multi-carrier (super-channel, SCh), distance-adaptive transmission of optical signals using flexibly assigned spectrum resources according to their demands [7].

In SS-FONs, lightpath connections are established using both spatial and spectral resources available in SDM links. A lightpath carries an SCh, which represents a bundle of optical signals transmitted using adjacent optical carriers within an appropriately allocated spectrum (frequency) slot. The lightpaths are routed between their source and destination nodes over the assigned spatial modes of SDM links. The allocation of frequency slots on spatial modes to particular lightpaths should be contention-free; i.e., any two lightpaths

cannot have assigned an overlapping segment of spectrum if they are routed through the same spatial mode over the same SDM link. The corresponding transmission resource allocation problem is called the routing, spatial mode and spectrum allocation (RSSA) problem [8].

One of the main issues in the operation of MCF-based SS-FONs is the degradation of signal quality of lightpaths due to the inter-core crosstalk effect that occurs in the MCFs [9]. In particular, the XT impairment affects the optical signals transmitted in an overlapping segment of spectrum in adjacent MCF cores. If the degradation is too high, the signals cannot be received properly. Therefore, the impact of XT on transmission quality should be accounted for when provisioning lightpaths in the SS-FONs connected using MCFs.

In this paper, we address the classical problem of planning of lightpath connections for a set of end-to-end traffic demands with a goal to optimize the utilization of spectral–spatial resources in MCF-based SS-FONs. The main novelty of this work is the application in network optimization of a reliable OSNR-based QoT estimation model [10], in which XT is considered as yet another source of the OSNR degradation, along with other physical-layer impairments (PLIs). The use of this model improves the accuracy of QoT estimation when compared to prior works concerning the optimization of SS-FONs, in which XT was considered either as the only source of signal degradation (e.g., see [11,12]), or it was treated independently from other PLIs (e.g., see [13,14]). To model the optimization problem considered, we propose a novel MIP formulation that incorporates the OSNR-based estimator as a set of problem variables and constraints. By solving MIP in different XT scenarios, we show that the use of the OSNR model complicates significantly the lightpath planning problem, which itself (i.e., without QoT awareness) is $\mathcal{NP}$-hard [8]. Therefore, to provide solutions to larger problem instances, we propose an efficient heuristic method. As numerical results show, the heuristic is capable of generating good-quality solutions to the optimization problem.

The main contributions of this work are the following:

1. Formulation of an MIP model for the lightpath planning problem that incorporates a reliable OSNR-based QoT estimator that accounts for the XT effect in MCFs;
2. Development of an efficient optimization method for solving the OSNR-aware lightpath planning problem;
3. Evaluation of the performance of the MIP model and the heuristic;
4. Analysis of the impact of XT on network performance in different network and MCF scenarios assuming the use of a reliable OSNR-based QoT model.

The rest of the paper is organized as follows. In Section 2, we discuss related works. In Section 3, we present the details of the network scenario and the OSNR model considered. In Section 4, we formulate the MIP optimization problem. In Section 5, we describe the optimization method. In Section 6, we present and discuss the numerical results. Finally, in Section 7, we conclude this work.

2. Related Works

The majority of optimization studies in SS-FONs have concerned the problem of lightpath provisioning for a set of traffic demands in static (offline) lightpath planning and for individual connection requests in dynamic (online) lightpath provisioning [8]. The lightpath provisioning problem in SS-FONs translates into the RSSA optimization problem, which was shown to be $\mathcal{NP}$-hard [8]. The RSSA-related optimization problems can be modeled as MIP problems [13,15–17]. MIPs yield exact, globally optimal solutions; however, their scalability is usually low, which means that they cannot provide even feasible solutions for larger RSSA problem instances in a reasonable time. Therefore, both heuristics [13,17–19] and meta-heuristics [13,19] have been proposed to generate solutions to large-scale RSSA problems. For more related works concerning the RSSA problem and the optimization of SS-FONs, we refer to our literature survey in [8].

Regarding the XT-aware optimization of SS-FONs, two main approaches were considered, namely: (a) avoidance of XT by means of specific spatial and spectral resource allocation

strategies [20,21] and (b) estimation of XT levels during the RSSA process [12,13,17,18,22,23]. The former approach does not guarantee that the XT levels of lightpaths are below the allowable thresholds. Therefore, these methods are not appropriate for highly loaded networks, in which the occupancy of spatial–spectral resources is dense. Contrarily, in the latter approach, the RSSA process is supported by the knowledge about the actual XT levels of both existing and potential (e.g., considered by an heuristic) lightpath allocations. In this scope, two basic methodologies for XT estimation were applied, namely: (a) worst-case XT [13,17,22,23] and (b) precise XT [12,14,18,24]. The worst-case XT estimation represents the maximum XT level that may occur in the MCF [13,14], or in particular cores [14], regardless of the state of the network. Although this method is simple, as the XT estimation is static and not dependent on lightpath allocations, still, it may lead to an inefficient use of resources due to overestimation of the actual XT levels, as shown in [14]. In contrast, the precise XT estimation approach accounts for the actual allocation of spatial and spectral resources in network links. The main disadvantage of this method is its computational effort, as any change in the network state involves the need for XT check for each potentially affected lightpath.

The estimation of transmission quality of lightpaths during the RSSA process, in order to verify whether they are acceptable, requires reliable analytical models. In many works concerning MCF-based SS-FONs (e.g., see [11,12,17,22,25,26]), the QoT verification is reduced to the estimation of crosstalk using the analytical model presented in [9]. Since these studies do not consider other linear and nonlinear physical-layer impairments that affect the transmission of optical signals in fibers, the accuracy of QoT estimation is limited in these works. In [13,14], an extended QoT model is used, which apart from using the model from [9] for XT verification, it accounts for the existence of other PLIs that may limit the maximum transmission reach (TR) of lightpaths in the network. However, in this approach, the QoT verification is still performed separately with regard to XT and other PLIs. Namely, first, it is checked whether the length of the lightpath is below the TR, and then crosstalk is estimated for this lightpath.

In fact, as discussed in [10], the XT impairment is a source of OSNR degradation and, therefore, it should be integrated with other PLIs in an OSNR-based model for reliable QoT estimation. In our recent work [24], we have used such an integrated OSNR model in a dynamic lightpath provisioning scenario. However, to the best of our knowledge, the application of this model in the optimization of SS-FONs has not been considered in the literature yet. This work aims at filling the gap by proposing an MIP formulation of the lightpath planning problem with the QoT constraints included and by developing an effective heuristic optimization method for solving the problem.

3. Network Scenario and QoT Model

3.1. General Assumptions

The spatially–spectrally flexible optical network that we consider in this study makes use of weakly coupled multi-core fiber links that carry optical signals transmitted as spectral super-channels. Each spectral SCh is formed by a group of optical carriers (OCs), which occupy an appropriately allocated frequency slot within a flexible frequency grid on the assigned MCF core. A frequency slot represents a subset of adjacent frequency slices on the frequency grid. We assume that guard bands are introduced between adjacent SChs for filtering and switching purposes.

The transmission and reception of OCs is realized using coherent transceivers. The transceivers operate at fixed band rates and generate OCs that occupy a fixed-width spectrum channel. The transceivers may use various modulation formats (MFs), and therefore, they can support different bit rates that depend on the spectral efficiency of the MFs. The MFs are selected based on the optical link properties. The OCs of a SCh use the same MF. Each SCh makes use of the required number of transceivers, according to the number of OCs it is composed of. In particular, if the bit rate of a traffic demand is above

the transceiver capacity, assuming the selected MF, this demand is realized in the network using several transceivers.

The lightpaths established in the network satisfy the spectrum and spatial continuity constraints. Namely, the spectrum continuity constraint imposes that the frequency slot assigned to the SCh carried by a lightpath does not change its routing path. The spatial continuity constraint means that a lightpath has assigned the same core in each MCF on the routing path. Spatial continuity simplifies the SDM switch architecture [27], and such an assumption is frequently used in the literature [8].

3.2. Quality of Transmission Model

To estimate the QoT of lightpaths, we make use of the incoherent noise accumulation model, as expressed by Equation (15) in [28], which is extended for the MCF-based SDM scenario by including the inter-core crosstalk [10]. This model assumes that noise increases linearly along the optical path, where XT is one of the sources of noise along with other linear and nonlinear physical layer impairments. According to this model, the QoT of a lightpath is acceptable if its signal-to-noise ratio (SNR) is above the SNR level required by the modulation format applied for this lightpath (denoted as SNR^{REQ}).

The SNR of lightpath l routed over path p consists of a number of links (indexed by e), where each link is composed of a number of fiber spans (indexed by i) and is calculated as:

$$SNR_l = \left(\sum_{e \in p} \left(\sum_{i \in e} \frac{P_i^{\mathrm{ASE}} + P_i^{\mathrm{NL}}}{P_{\mathrm{ch}}} + \mu_e^{\mathrm{XT}} \right) \right)^{-1}, \tag{1}$$

where P_{ch}, P_i^{ASE}, and P_i^{NL} denote the signal, EDFA noise, and nonlinear noise powers per channel in fiber span i, respectively, and μ_e^{XT} is the crosstalk coefficient in link e. We consider that the channel power is optimized locally for individual links, which leads to the global optimization of QoT in the network according to [29]. The optimal channel power is calculated from $P_{\mathrm{ASE}} = 2P_{\mathrm{NL}}$ constraint [28], which is also valid for the extended model including XT.

In Equation (1), the value of crosstalk coefficient μ_e^{XT} is calculated according to [9] as:

$$\mu_e^{\mathrm{XT}} = L_e \cdot K_e \cdot 10^{\left(XT^{\mathrm{REF}} + XT^{\mathrm{MARGIN}}\right)/10}, \tag{2}$$

where L_e is the length of link e, K_e is the number of adjacent cores that cause crosstalk in a given core and in a given spectrum band in link e, XT^{REF} denotes the reference level of XT between two adjacent cores in a given MCF (expressed in [dB/km]), and XT^{MARGIN} is an extra margin with which XT is estimated; according to [9], we consider $XT^{\mathrm{MARGIN}} = 8$ dB for quantile $q = 0.9999$.

In Equation (2), the value of K_e reflects the actual maximum occupancy of cores that are adjacent to a given core assigned to lightpath l, which is in accordance to the precise XT methodology used in [14]. Namely, if lightpath l uses frequency slices $F = (s_1, ..., s_S)$ and $K_{e,s}$ is the number of allocated cores adjacent to a given core in link e on slice s, then we have $K_e = \max_{s \in F} \{K_{e,s}\}$.

In order to apply nonlinear Model (1) in an MIP formulation (in Section 4), we transform it as the following. Firstly, we consider the inverse of SNRs instead of direct SNR values, which leaves us with the summation operator on the right-hand side of Equation (1). Secondly, since the values of P_{ch}, P_i^{ASE}, and P_i^{NL} are static and do not depend on the actual load of neighbor MCF cores, we represent the summation of the quotient of these power values by means of static parameter $\beta(e)$, which is pre-calculated for each network link e. Eventually, we substitute coefficient μ_e^{XT} in Equation (1) with Equation (2) and represent the factors that do not depend on MCF link load by means of static parameter $\gamma(e)$, which is specific for each link e. As a result, we obtain the following relation:

$$SNR_l^{-1} = \sum_{e \in p} (\beta(e) + \gamma(e) \cdot K_e), \tag{3}$$

where

$$\beta(e) = \sum_{i \in e} \left(P_i^{\mathrm{ASE}} + P_i^{\mathrm{NL}} \right) \cdot P_{\mathrm{ch}}^{-1}, \tag{4}$$

$$\gamma(e) = L_e \cdot 10^{\left(XT^{\mathrm{REF}} + XT^{\mathrm{MARGIN}} \right)/10}. \tag{5}$$

Due to the inverse operation, we consider that the QoT of a lightpath is acceptable whenever the value calculated using Equation (3) does not exceed the inverse of the required SNR value, which we denote as Q, where $Q = (SNR^{\mathrm{REQ}})^{-1}$.

In Figure 1, we compare Model (1), referred to as *OSNR-based*, with the QoT model considered in previous networking studies in SS-FONs (e.g., in [11–14]) that are based on the estimation of XT only [9] and which we refer to as the *XT-based* approach. In particular, we show transmission reach values estimated using both models (on the left side) and a relative difference in the estimated TR values (on the right side) for different numbers of active adjacent cores (K) in a function of the reference XT level in MCF (XT^{REF}), assuming the QPSK modulation format. We can see that the TR obtained using the XT-based model may be much higher than when applying the OSNR-based model. Indeed, the relative difference in TRs may reach up to between 80% and 100% for some XT^{REF} values (around -61 dB/km for $K = 6$ and -57 dB/km for $K \in \{2, 3\}$). This difference is significant and may result in improper network operation if the less conservative XT-based model is used.

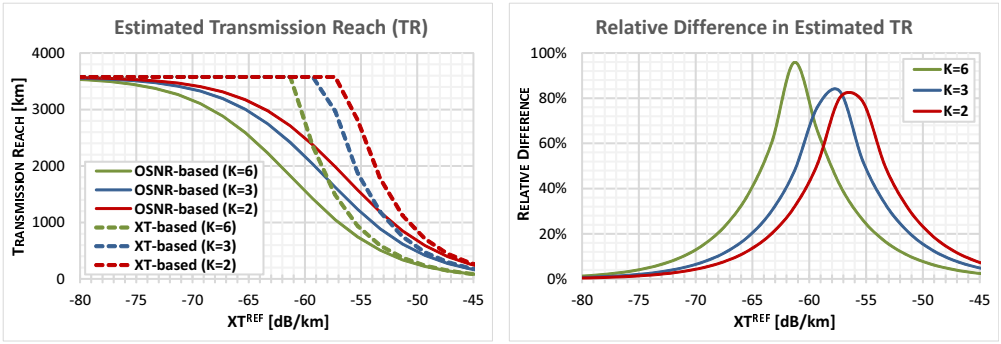

Figure 1. Comparison of estimated transmission reaches in a function of crosstalk level for OSNR-based and XT-based QoT models assuming QPSK modulation format.

Therefore, in the remainder of the paper, we focus on application of the OSNR-based QoT model in the optimization of SS-FONs, namely, on mathematical modeling of the OSNR-aware lightpath planning problem and on developing an effective optimization method for solving it.

4. MIP Problem Formulation

In this section, we formulate the optimization problem that we aim to solve, namely, the OSNR-aware lightpath planning problem in MCF-based SS-FONs. The problem concerns the establishment of lightpath connections for a set of traffic demands in such a way that any spectrum segment of any core of an MCF link is assigned to one lightpath at most and each lightpath satisfies the SNR requirement discussed in Section 3.2. Following the assumption in Section 3, each lightpath has assigned a unique MCF core index, which is the same for each link of its routing path. In addition, the frequency slot assigned to a lightpath does not change in consecutive links of the path. In other words, the spatial and spectral continuity constraints are imposed. The optimization goal is to minimize the maximum spectrum usage, which is defined as the width of spectrum required to serve all demands.

To formulate the optimization problem as an MIP problem, we introduce the notation presented in Table 1. In addition, in Table 1, we define a set of problem variables that we use to model the MIP problem.

Table 1. Notation.

Sets and Parameters	
$\mathcal{V}$	set of SDM optical nodes
$\mathcal{E}$	set of MCF links
$\mathcal{C}$	set of cores available at each MCF link
$\mathcal{C}(c)$	set of cores adjacent to core c
$\mathcal{S}$	set of frequency slices of a fixed width; $\mathcal{S} = \{s_1, s_2, \ldots, s_{\lvert\mathcal{S}\rvert}\}$
$\mathcal{M}$	set of available modulation formats
$\mathcal{D}$	set of traffic demands
$\mathcal{L}(d)$	set of allowable lightpaths for demand d
$\mathcal{L}$	set of all allowable lightpaths; $\mathcal{L} = \cup_{d\in\mathcal{D}}\mathcal{L}(d)$
$\mathcal{L}(e,c,s)$	set of lightpaths routed through link e, core c, and slice s
$\mathcal{E}(l)$	set of links belonging to the routing path of lightpath l; $\mathcal{E}(l) \subseteq \mathcal{E}$
$\mathcal{S}(l)$	set of frequency slices assigned to lightpath l; $\mathcal{S}(l) \subseteq \mathcal{S}$
$c(l)$	core assigned to lightpath l; $c(l) \in \mathcal{C}$
$m(l)$	modulation format used by lightpath l; $m(l) \in \mathcal{M}$
$d(l)$	demand realized by lightpath l
$Q(m)$	the inverse of the required SNR value for modulation format m
Variables	
x_{dl}	binary, equal to 1 if lightpath $l \in \mathcal{L}(d)$ is selected for demand $d \in \mathcal{D}$
y_{ecs}	binary, equal to 1 if slice $s \in \mathcal{S}$ of core $c \in \mathcal{C}$ of link $e \in \mathcal{E}$ is used be a lightpath
y_s	binary, equal to 1 if slice $s \in \mathcal{S}$ is used in the network
w_{ecs}	continuous, represents the inverse of the SNR value in slice $s \in \mathcal{S}$ of core $c \in \mathcal{C}$ of link $e \in \mathcal{E}$

The MIP formulation is as follows:

$$\text{minimize } z = \sum_{s\in\mathcal{S}} y_s, \tag{6}$$

$$\sum_{l\in\mathcal{L}(d)} x_{dl} = 1, \qquad d \in \mathcal{D}, \tag{7}$$

$$\sum_{l\in\mathcal{L}(e,c,s)} x_{d(l)l} = y_{ecs}, \qquad e \in \mathcal{E}, c \in \mathcal{C}, s \in \mathcal{S}, \tag{8}$$

$$y_{ecs} \leq y_s \qquad e \in \mathcal{E}, c \in \mathcal{C}, s \in \mathcal{S}, \tag{9}$$

$$\beta(e) + \gamma(e) \cdot \sum_{c'\in\mathcal{C}(c)} y_{ec's} = w_{ecs}, \qquad e \in \mathcal{E}, c \in \mathcal{C}, s \in \mathcal{S}, \tag{10}$$

$$\sum_{e\in\mathcal{E}(l)} w_{ec(l)s} \leq Q(m(l)) + (1 - x_{dl}) \cdot B, \qquad d \in \mathcal{D}, l \in \mathcal{L}(d), s \in \mathcal{S}(l). \tag{11}$$

Optimization objective (6) minimizes the number of frequency slices that are actually used in the network (calculated as the sum of variables y_s). Constraint (7) assures that each demand will be realized using exactly one lightpath selected from the set of allowable lightpaths. Constraint (8) assures that the selected lightpaths do not collide with each other; namely, each slice on each core of each link can be used by one lightpath at most since y_{ecs} is a binary variable. Constraint (9) defines variables y_s that indicates whether slice s is used on at least one link. Eventually, Constraints (10) and (11) implement Model (3) for assuring QoT. Constraint (10) estimates the inverse value of SNR for each slice on each core of each link, taking into account the allocation status in neighbour cores (the sum of variables y_{ecs}). Constraint (11) assures that whenever lightpath l is selected for demand d (i.e., if $x_{dl} = 1$), the sum of inverse SNR values (variables w_{ecs}) corresponding to the spectral–spatial resources used by lightpath l on its routing path does not exceed the limit allowable for the modulation format used by this lightpath (i.e., value $Q(m(l))$), according to Model (3). B represents a large value that assures that Constraint (11) is always satisfied if variable x_{dl} is equal to 0.

Solving MIP model (4) is difficult even without the presence of OSRN constraints (10)–(11) [30]. Therefore, in the next section, we propose an efficient heuristic method for generating good-quality solutions to larger instances of the optimization problem considered.

5. Optimization Method

In this section, we propose an optimization method for the OSNR-aware lightpath planning problem in MCF-based SS-FONs. The optimization method applies the OSNR-based QoT estimation model presented in Section 3.2 and generates feasible solutions to the MIP model formulated in Section 4. In the description of the method, we apply the notation presented in previous sections, and we introduce additional symbols specific to the algorithm.

The core element of the optimization method is the OSRN-aware lightpath allocation (OSNR-LA) algorithm, which solves the problem of allocation of lightpaths satisfying given SNR requirements for an ordered set of traffic demands (denoted as $\widetilde{\mathcal{D}}$), which are processed one by one. The algorithm makes use of candidate routing paths $\mathcal{P}(d)$ that are available for each demand d. In OSNR-LA, the verification of SNR is performed both for each candidate lightpath and for all already allocated and possibly affected lightpaths based on the actual allocation status of spectral–spatial resources in network links, which is maintained in a network state matrix A. In particular, the allocation status of frequency slices in cores of particular network links is represented using the maximal free-occupied block (MFOB) approach proposed in [30] that utilizes a three-dimensional matrix $A^{|\mathcal{E}|\times|\mathcal{C}|\times|\mathcal{S}|}$. Element $A(e,c,s)$ corresponds to slice s in core c of link e, and it represents the allocation status of slice s (free or busy) as well as contains the information about how many consecutive slices (beginning from s) have the same status as slice s. By reading element $A(e,c,s)$, the algorithm is able to determine either whether the requested number of consecutive slices is available for allocation of a lightpath or which slice is worth checking next. As shown in [30], the application of MFOB speeds up considerably the searching for free spectrum resources.

A pseudo-code of the OSNR-LA algorithm is shown in Algorithm 1. In lines 1 and 2, spectral–spatial resource allocation state matrix (A), the set of allocated lightpaths ($\overline{\mathcal{L}}$), and the required number of slices (z) are initialized. In line 3, a loop iterating over consecutive demands from the ordered set of demands ($\widetilde{\mathcal{D}}$) begins. In line 4, the best lightpath ($\bar{l}$) selected for demand d is initialized. In lines 5 and 6, respectively, loops iterating over candidate paths ($\mathcal{P}(d)$) for demand d and available MCF cores ($\mathcal{C}$) are started. The beginning frequency slice (s_{beg}) of a candidate lightpath is initialized in line 7, and a "while" loop iterating over consecutive candidate slices starts in line 8. In line 9, frequency slot f beginning from slice s_{beg} and occupying $N(d,p,c)$ consecutive slices is initialized. Here, $N(d,p,c)$ represents the number of slices required to serve the bit rate of demand d on path p and core c, assuming that the best modulation format that can be used on path p is selected. In line 10, candidate lightpath l is initialized with path p, core c, and frequency slot f. In line 11, it is checked using the allocation state matrix (A) whether spectral resources are available for lightpath l in core c in each link of path p. If the resources are available, then subset $\widetilde{\mathcal{L}}$ of the already selected lightpaths ($\widetilde{\mathcal{L}} \subseteq \overline{\mathcal{L}}$) that might be affected by lightpath l is determined in line 12. In line 13, it is checked whether lightpath l and all possibly affected lightpaths ($\widetilde{\mathcal{L}}$) satisfy the QoT requirement by calculating their inverse SNR values, using Model (3), and comparing them with allowable limits, as discussed in Section 3.2. If the QoT of lightpaths is acceptable, then it is checked (in line 14) whether candidate lightpath l has a lower beginning slice index than the best lightpath ($\bar{l}$) found so far for demand d. If so, lightpath $\bar{l}$ is substituted with lightpath l (in line 15) and the "while" loop is terminated (in line 16). Otherwise, if either spectral resources are not available or the QoT of some lightpath is not satisfied, then beginning slice s_{beg} is updated to the next available slice (in line 18), and the candidate lightpath verification procedure (starting in line 9) is repeated. After all candidate path–core pairs have been processed, the best lightpath ($\bar{l}$) found for demand d is included into the set of allocated lightpaths ($\overline{\mathcal{L}}$) and network state (A) is updated in line 19. In addition, in line 19, the required number of frequency slices (z) is updated if the ending slice (s_{end}) of lightpath $\bar{l}$ exceeds z. The algorithm terminates after all demands have been processed.

Algorithm 1 OSNR-Aware Lightpath Allocation (OSNR-LA)

Require: ordered demands $\widetilde{\mathcal{D}}$, candidate paths $\mathcal{P}$

Initialize resource allocation state matrix A
Allocated lightpaths $\overline{\mathcal{L}} \leftarrow \emptyset$, required number of slices $z \leftarrow 0$
for all demand $d \in \widetilde{\mathcal{D}}$ **do**
    best lightpath $\bar{l} \leftarrow \emptyset$
    for all path $p \in \mathcal{P}(d)$ **do**
        for all core $c \in \mathcal{C}$ **do**
            frequency slice $s_{beg} \leftarrow 1$
            while $(s_{beg} \leq |\mathcal{S}|)$ **do**
                frequency slot $f \leftarrow (s_{beg}, s_{beg} + N(d,p,c) - 1)$
                lightpath $l \leftarrow (p,c,f)$
                if spectral resources are available in A for lightpath l **then**
                $\widetilde{\mathcal{L}} \leftarrow$ the lightpaths from $\overline{\mathcal{L}}$ that have a common link and a common slice and are carried on a neighbor core to l
                if QoT estimated using Equation (3) is acceptable for all lightpaths in $\{l\} \cup \widetilde{\mathcal{L}}$ **then**
                if $\bar{l} = \emptyset \vee s_{beg}(\bar{l}) > s_{beg}$ **then**
                $\bar{l} \leftarrow l$
                break
            else
                $s_{beg} \leftarrow$ next available slice obtained from A
    Include lightpath $\bar{l}$ into $\overline{\mathcal{L}}$, update network state in A, and update $z \leftarrow \max\{z, s_{end}(\bar{l})\}$

Ensure: lightpaths $\overline{\mathcal{L}}$ satisfying QoT for demands in $\mathcal{D}$, the number of required slices (z)

Algorithm 1 returns a feasible allocation of lightpaths after processing the demands according to given order ($\widetilde{\mathcal{D}}$). Since the lightpaths selected and spatial–spectral resources allocated may differ for different sequences of processed demands, the value of objective function (z), which represents the number of frequency slices required in the network, may differ as well. Therefore, as the value of z is subject to minimization, we execute Algorithm 1 a number of times, each time assuming a different order od demands $\widetilde{\mathcal{D}}$, and we consider the solution with the lowest value of z as the best one and returned by the optimization method.

To drive the algorithm in its search toward the best order of demands, we apply a simulated annealing (SA) method [31]. Namely, at each SA iteration, two randomly selected demands in $\widetilde{\mathcal{D}}$ are swapped, and Algorithm 1 is executed for the resulting order of demands. If the obtained value of z is improved, it is considered as the best one and order $\widetilde{\mathcal{D}}$ is accepted as the current one; otherwise, order $\widetilde{\mathcal{D}}$ is accepted with certain probability, which decreases after each SA iteration. To control the performance of SA, two parameters are used: temperature $\mathcal{T} > 0$ determining the probability of accepting non-improving solutions and cooling rate ρ representing the speed of decreasing the temperature in consecutive iterations, where $0 < \rho < 1$. We consider that $\mathcal{T}$ is initialized with the product of the value of z obtained in the first algorithm iteration and a temperature coefficient (denoted as τ). After each SA iteration, $\mathcal{T}$ is updated and takes the value $\mathcal{T} \times \rho$. The probability of accepting non-improving solutions is calculated as $e^{-(z-\bar{z})/\mathcal{T}}$, where z and $\bar{z}$ are objective function values corresponding, respectively, to the new and current solution. In Section 6.2, we perform algorithm tuning to select the values of τ and ρ that offer the best performance.

Eventually, to speed up the algorithm, we make use of multi-core CPU capabilities and run a number of parallel threads (one per a logical CPU core), where each thread executes an instance of the SA method described above. For algorithm parallelization, we apply the cooperative with solution exchange (CSE) approach proposed in [30]. In CSE, the best global solution (namely, best order $\widetilde{\mathcal{D}}$ and best value of z) is shared between the threads. Whenever improved, this best global solution is updated and distributed among the parallel instances of SA that consider $\widetilde{\mathcal{D}}$ as the current order of demands. As shown

in [30], a parallel simulated annealing (PSA) algorithm allows significantly decreasing computation times.

In the next section, we analyze the performance of the above presented OSNR-aware lightpath planning method—referred to as OSNR-LA-PSA—by means of numerical experiments run in various network scenarios.

6. Numerical Results

We evaluate the proposed MIP optimization model and the OSNR-LA-PSA method in three different networks: generic German (DT12), Spanish (TEL30), and European (EURO16), which are shown in Figure 2. The parameters of network topologies are summarized in Table 2.

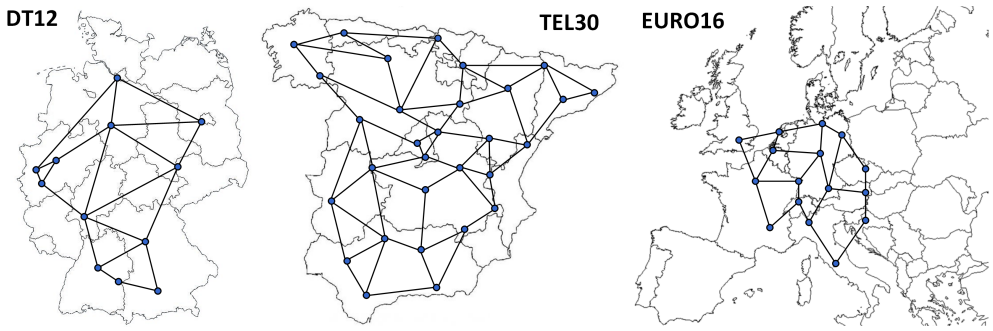

Figure 2. Network topologies: DT12, TEL30, and EURO16.

Table 2. Characteristics of network topologies; SP means shortest path.

Network	Nodes	Links	Length [km]			
			Mean Link	Mean SP	Max SP	Max Path
DT12	12	40	243	483	1019	2056
TEL30	30	112	148	450	944	1130
EURO16	16	46	486	1185	2663	4781

The flexible frequency grid has a 12.5 GHz granularity. We assume that each network link consists of a number of 100 km length spans and a residual span that complements the link according to its actual length. The candidate routing paths are generated using a *k*-shortest path algorithm. We assume that *k* candidate paths are available for each pair of nodes. The paths are ordered according to their ascending physical lengths. In Section 6.1, we study the impact of *k* on network performance with the aim to select such *k* that offers a good tradeoff between the obtained results and algorithm runtimes. We consider two MCFs (shown in Figure 3): a typical seven-core hexagonal weakly coupled MCF that consists of a central core and six regularly spaced outer cores (MCF-7) and a six-core MCF that lacks the central core (MCF-6).

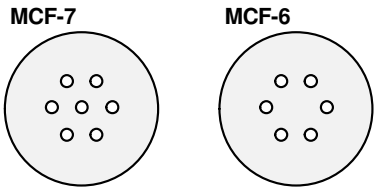

Figure 3. Tested fibers: MCF-7 and MCF-6.

The optical carrier and the guard-band occupy, respectively, *three* and *one* frequency slices. Four modulation formats are considered: BPSK, QPSK, 8QAM, and 16QAM, with the carried bit rate of 50, 100, 150, and 200 Gbit/s per 32 GBd OC, respectively. Traffic demands have randomly generated end nodes, and bit rates were uniformly distributed between 50 Gbit/s and 1 Tbit/s with a 50 Gbit/s granularity.

The levels of crosstalk depend on the design and physical properties of MCFs [9]. Different values of crosstalk are mentioned in the literature, and the latest measurements in a recirculating loop for PDM–16QAM signals estimate it between −57 and −60 dB/km [32]. Low XT levels are difficult to be achieved in a seven-core MCF of standard 125 µm diameter due to low outer cladding thickness, which increases excess loss [33]. Therefore, we study the MCF scenarios in which the level of XT between two adjacent cores (XT^{REF}), i.e., due to signal leaking from one core to another core, is between −51 and −61 dB/km. Such values display the highest differences between the conventional XT-based model and the considered OSNR-based model (as shown in Figure 1) and, at the same time, have a significant impact on the transmission reach.

As a reference, we consider an SDM scenario in which XT is not present (denoted by "∞"), which might correspond to a network using single-mode fiber bundles (SMFB) [8]. The transmission model uses the assumptions formulated in Section 3. The system parameters and the required SNR levels for the MFs considered [34] are shown in Table 3.

Table 3. Transmission system parameters.

Attenuation coefficient (α) (dB/km)	0.21
Chromatic dispersion (CD) (ps/nm/km)	16.7
Nonlinear index (n_2) ($\mathrm{W}^2/\mathrm{m}^{-1}$)	2.3×10^{-20}
Effective area (A_{eff}) ($\mu\mathrm{m}^2$)	80
EDFA noise figure (NF) (dB)	5
Required SNR for BPSK (dB)	6.8
Required SNR for QPSK (dB)	9.8
Required SNR for 8QAM (dB)	14.3
Required SNR for 16QAM (dB)	16.5

The evaluation was performed on a 3.7 GHz 32-core Ryzen Threadripper-class machine (64 logical threads) with 64 GB RAM. The CPLEX solver v.12.9 [35], run with default settings in a parallel mode, was used to solve the MIP model.

6.1. Impact of Candidate Routing Paths

We started by analyzing the impact of the amount of available candidate paths (k) on OSNR-LA-PSA performance. We assumed $\tau = 1$, $\rho = 0.9$, and 10^5 iterations in OSNR-LA-PSA. The evaluation was performed for $|\mathcal{D}| \in \{100, 150, 200\}$ and for both fiber types, assuming $XT^{\mathrm{REF}} \in \{-51, -57, -61\}$ dB/km. In particular, for each k and network topology, we obtained results for 18 different scenarios, which we averaged afterwards.

In Table 4, we show average values of objective function (z) and algorithm running time (T) for different numbers of candidate paths (k) in each network. We can see that z can be improved considerably when increasing k. However, starting from some value of k, the improvement is either none or negligible, while the algorithm runtimes still increase. Therefore, in the remainder of the paper, we assume that k is equal to 6, 8, and 5, respectively, for DT12, TEL30, and EURO16, which is a good tradeoff between the obtained results and algorithm runtimes.

6.2. Tuning of OSNR-LA-PSA Method

In order to tune the OSNR-LA-PSA method, we executed it assuming different values of cooling rate ρ and initial temperature coefficient τ, where $0.8 \leq \rho \leq 0.999$ and $0.1 \leq \tau \leq 10$. For each pair of ρ and τ, we evaluated 20 different problem instances, namely, 10 randomly generated demand sets for each MCF scenario (MCF-6 and MCF-7), assuming $|\mathcal{D}| = 200$, $XT^{\mathrm{REF}} = -57$ dB/km, and 10^4 algorithm iterations. Next, the results were averaged.

Table 4. An average value of objective function (z) and algorithm processing times (T) for different number of candidate paths (k); T in seconds.

k	DT12		TEL30		EURO16	
	z	T	z	T	z	T
1	58.3	5	44.7	6	79.1	7
2	53.3	9	35.9	10	63.1	12
3	48.7	13	32.8	14	61.1	19
4	45.4	18	32.2	18	61.1	25
5	44.4	22	31.1	23	60.8	31
6	43.9	26	30.5	28	60.8	37
8	43.8	36	29.8	35	60.9	50
10	43.8	44	29.7	42	61.0	63

In Table 5, we present the average values of z in a function of the OSNR-LA-PSA parameters in the studied networks. Although the results do not differ much, still, the best performance (i.e., the lowest value of z) is achieved for $\rho = 0.9$ and $\tau = 1$ in each network. Therefore, we apply these best values of ρ and τ in the following sections.

Table 5. Results of tuning process—an average value of objective function (z) for different values of initial temperature coefficient (τ) and cooling rate (ρ) in analyzed networks; best values marked in bold.

ρ	τ (DT12)					τ (TEL30)					τ (EURO16)				
	0.1	**0.5**	**1**	**5**	**10**	**0.1**	**0.5**	**1**	**5**	**10**	**0.1**	**0.5**	**1**	**5**	**10**
0.8	55.0	55.0	55.1	55.6	54.8	35.5	35.5	35.3	35.5	35.6	74.8	74.8	74.3	74.3	74.0
0.85	55.5	54.9	55.0	55.2	55.1	35.5	35.2	35.2	35.4	35.2	74.7	74.3	74.2	74.3	73.9
0.9	54.9	55.0	**54.7**	54.9	55.1	35.6	35.4	**35.1**	35.4	35.4	74.2	74.5	**73.5**	73.9	74.2
0.99	55.8	56.3	56.0	55.8	55.9	35.7	36.5	36.1	36.4	36.3	75.2	75.5	75.6	76.3	75.8
0.999	55.7	55.9	56.1	55.9	56.1	35.9	36.3	36.3	36.3	36.3	75.8	75.8	75.7	75.8	76.1

6.3. Performance of OSNR-LA-PSA vs. MIP Model

To evaluate the quality of solutions generated by the OSNR-LA-PSA method, we compared these solutions with the results obtained by solving the MIP model presented in Section 4 using the CPLEX solver. The analysis was performed in different routing, traffic, and XT scenarios in network DT12. Namely, we considered $k \in \{1, 3\}$ candidate routing paths, $|\mathcal{D}| \in \{50, 80, 100\}$ demands, and reference XT levels $XT^{\text{REF}} \in \{-51, -57, -\infty\}$ dB/km. CPLEX was run with a 1 h runtime limit, while 10^5 iterations were performed in OSNR-LA-PSA. Our main focus was on the objective function values z^{MIP} and $z^{\text{OSNR-LA-PSA}}$ as well as on computation times T^{MIP} and $T^{\text{OSNR-LA-PSA}}$ obtained, respectively, using the MIP model and the OSNR-LA-PSA method.

The obtained results are presented in Table 6. Apart from the above-mentioned metrics, we report the MIP optimality gaps (Δ^{MIP}) and the performance gaps between both methods (Δ^{rel}). Namely, Δ^{MIP} expresses a relative difference between z^{MIP} and CPLEX lower bounds after the 1 h computation period, while Δ^{rel} represents a relative difference between the obtained values of z^{MIP} and $z^{\text{OSNR-LA-PSA}}$.

First of all, we can see that the presence of crosstalk complicates extremely solving the MIP model. While CPLEX is able to find optimal solutions ($\Delta^{\text{MIP}} = 0\%$) in a few seconds in the XT-less scenario ($-\infty$ dB/km), it does not achieve the goal in most cases for higher values of XT^{REF}. Indeed, even for one candidate routing path ($k = 1$) and $|\mathcal{D}| = 80$ demands, the MIP optimality gap is above 20%, and it increases for higher values of k and $|\mathcal{D}|$; for $k = 3$ and $|\mathcal{D}| = 100$, a feasible solution could not be found within the 1 h runtime limit.

Table 6. Comparison of MIP and OSNR-LA-PSA performance in different routing, traffic and crosstalk scenarios in network DT12; T^{MIP} and $T^{\text{OSNR-LA-PSA}}$ in seconds.

Scenario			MIP Results			OSNR-LA-PSA Results		Difference in z
k	$\lvert\mathcal{D}\rvert$	XT^{REF}	z^{MIP}	Δ^{MIP}	T^{MIP}	$z^{\text{OSNR-LA-PSA}}$	$T^{\text{OSNR-LA-PSA}}$	Δ^{rel}
1	50	$-\infty$	16	0%	0.1	16	0.3	0%
		-57	17	0%	216	17	1.5	0%
		-51	26	0%	867	26	1.0	0%
	80	$-\infty$	19	0%	1.3	19	0.4	0%
		-57	26	23%	3600	26	2.4	0%
		-51	37	43%	3600	36	1.7	-3%
	100	$-\infty$	23	0%	2.6	23	0.5	0%
		-57	47	51%	3600	37	3.7	-21%
		-51	52	56%	3600	49	3.2	-6%
3	50	$-\infty$	16	0%	2.0	16	0.3	0%
		-57	16	0%	2994	16	3.3	0%
		-51	20	20%	3600	20	2.4	0%
	80	$-\infty$	19	0%	3.8	19	0.5	0%
		-57	27	30%	3600	20	6.9	-26%
		-51	37	49%	3600	26	5.7	-30%
	100	$-\infty$	22	0%	8.1	22	0.7	0%
		-57	unknown	–	3600	32	10.5	–
		-51	unknown	–	3600	44	7.4	–

At the same time, OSNR-LA-PSA solutions are obtained in very short times, not exceeding about 10 seconds, for all evaluated problem instances. The OSNR-LA-PSA results ($z^{\text{OSNR-LA-PSA}}$) are either the same or better (lower) than the MIP results (z^{MIP}). In particular, whenever MIP solutions are optimal (i.e., $\Delta^{\text{MIP}} = 0\%$), the solutions found using OSNR-LA-PSA have the same objective value and, thus, are also optimal. Moreover, in several cases when the optimality of MIP solutions is not confirmed ($\Delta^{\text{MIP}} > 0\%$), OSNR-LA-PSA achieves much better results than MIP (within its runtime limit), where the relative difference Δ^{rel} between the feasible solutions found reaches up to -30%. Note that a negative Δ^{rel} signifies that $z^{\text{OSNR-LA-PSA}} < z^{\text{MIP}}$.

The above results show that the MIP model has a low scalability, especially, at the presence of crosstalk. Concurrently, the processing times of the OSNR-LA-PSA method are low and the quality of solutions generated is high in the network scenarios evaluated. These results indicate that OSNR-LA-PSA is an effective and efficient method for solving the OSNR-aware lightpath planning problem. Therefore, in the next section, we apply this method for analysis of larger network and traffic scenarios.

6.4. Evaluation of Network Performance

The last set of experiments was aimed at analyzing network performance in larger network scenarios that differ in topology, traffic demands, crosstalk levels, and MCFs used. The results were obtained after 5×10^5 iterations performed in the OSNR-LA-PSA method.

In Figure 4, we present the number of used slices (z) in the SS-FON network using fiber MCF-7 after optimized planning of lightpaths for $|\mathcal{D}|$ demands, assuming different topologies and XT levels. We can see that z increases with $|\mathcal{D}|$, which is obvious as higher traffic demands result in higher bandwidth (spectrum) requirements. The smallest spectrum requirements are in network TEL30, which is due to both a larger number of links and shorter paths in this topology than in the other two networks (see Table 2). Indeed, the average link load is lower in a network with a larger number of links, while shorter paths enable the application of spectrally efficient modulation formats. The highest values of z are observed in EURO16, which is due to long transmission paths and, consequently, less efficient MFs that can be applied in this network. In Figure 4, we can also see that higher

XT levels result in higher spectrum requirements. This can be explained by the fact that the allocation of lightpaths on neighbor MCF cores that would be acceptable in a low XT scenario might not be permitted in a high XT scenario due to an excessive degradation of QoT. In such a case, the lightpaths might need to be allocated within non-overlapping frequency ranges, thus increasing the spectrum requirements.

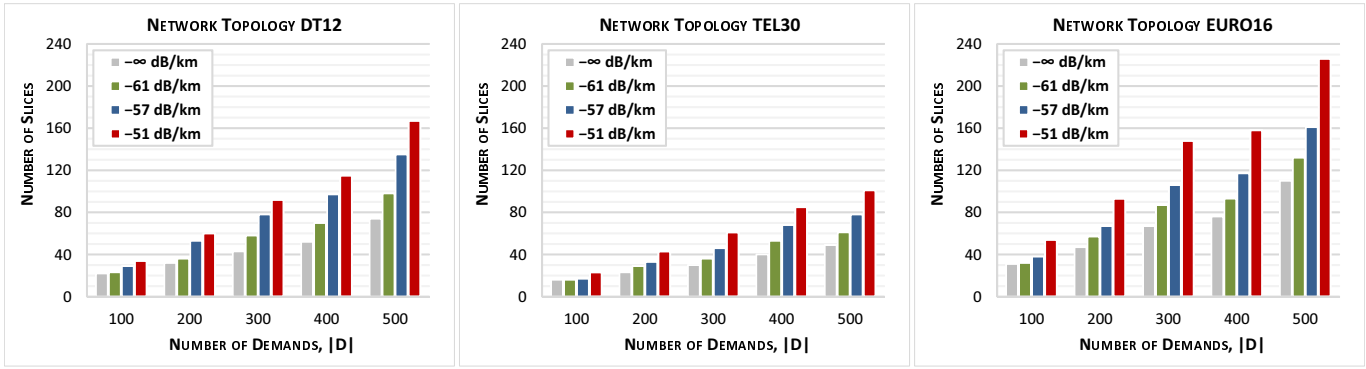

Figure 4. The required number of slices in a function of the number of demands in different network and crosstalk scenarios assuming fiber MCF-7.

In Figure 5, we show a relative difference in the number of used slices (δ) for particular XT scenarios with respect to the SDM scenario in which XT is not present ($XT^{\mathrm{REF}} = -\infty$). The value of δ increases with the number of demands up to some level at which it stabilizes. In addition, in each network, we can see that the higher the XT level, then the higher the value of δ. In particular, the spectrum requirements of the MCF-based network with a high level of XT ($XT^{\mathrm{REF}} = -51$ dB/km) might be more than twice as much as of the network connected using SMFB links. In general, the values of δ are on comparable levels in different network topologies for particular XT levels.

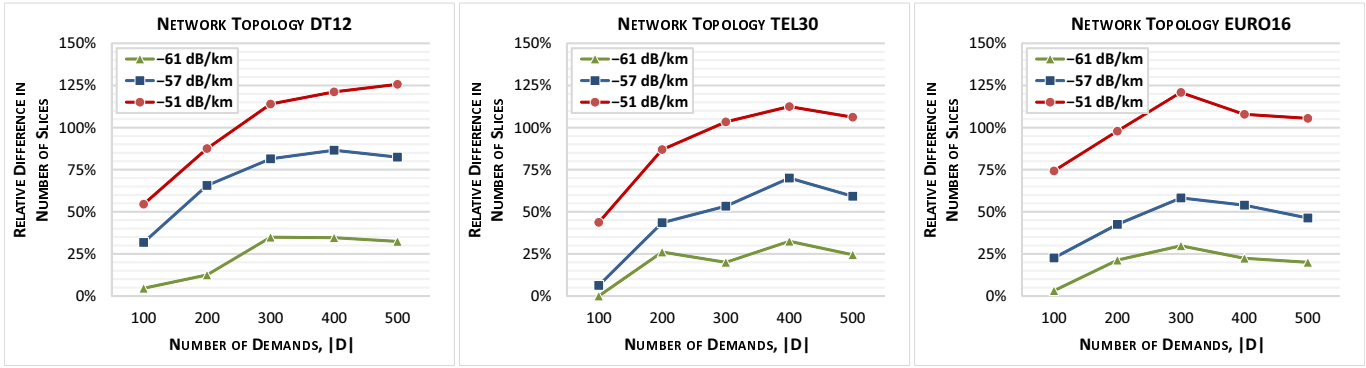

Figure 5. Relative difference in the number of required slices with respect to the XT-less SDM scenario as a function of the number of demands in different network and crosstalk scenarios assuming fiber MCF-7.

In Figure 6, we analyze the impact of the types of multi-core fiber used, namely, MCF-6 and MCF-7, on spectrum requirements in different XT scenarios. The bars represent the number of slices (z) required to allocate $|\mathcal{D}| = 500$ demands, while the lines reflect the relative difference (δ) in the number of slices required in the MCF-6 scenario when compared to the MCF-7 case. We can see that in the XT-less scenario ($XT^{\mathrm{REF}} = -\infty$), the networks take advantage of an additional core that is available in MCF-7 and utilize between about 14% (in TEL30) and 17% (in EURO16) spectrum resources less than in the case of MCF-6. However, if crosstalk is present, the gain in spectrum usage drops considerably down, to about 1%–2%, in all networks. In smaller networks DT12 and TEL30, it happens for $XT^{\mathrm{REF}} = -61$ dB/km, while in EURO16, it is observed for $XT^{\mathrm{REF}} = -57$ dB/km. The

MCF-6 differs from MCF-7 only in the lack of the central core (see Figure 3). Note that this core is the one most affected by XT as it is adjacent to all six outer cores. Therefore, this core is likely to be utilized less if XT is present. As a consequence, it reduces the potential performance gain from the higher capacity available in MCF-7 when compared to MCF-6, which is reflected in the results in Figure 6.

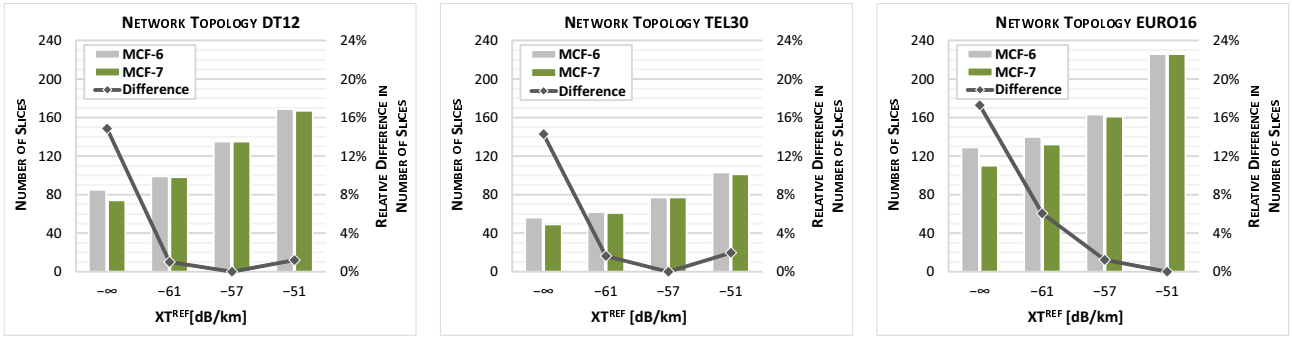

Figure 6. Comparison of network performance for fibers MCF-6 and MCF-7 in different network and crosstalk scenarios assuming $|\mathcal{D}| = 500$: the required number of slices (bars) and relative difference in the number of required slices between both MCF options (lines).

Eventually, in Figure 7, we report the computation times of the OSNR-LA-PSA method as a function of the number of processed demands for $XT^{\mathrm{REF}} = -57$ dB/km (left chart) and the crosstalk level for $|\mathcal{D}| = 500$ (right chart), assuming MCF-7 and 5×10^5 algorithm iterations. We can see that the algorithm runtimes increase almost linearly with $|\mathcal{D}|$. At the same time, the presence of XT has a huge impact on algorithm computation times when compared to the XT-less scenario. This is mainly due to the need for a frequent, dynamic verification of QoT for every slice of each lightpath possibly affected by XT, which is a time-consuming process. Note that in a XT-less scenario, this process can be omitted, since the QoT estimation for particular lightpaths is static and not dependent on the actual allocation of spectral-spatial resources in the network. In addition, note that the application of both the proposed MFOB resource allocation approach and parallel processing in the optimization method (see Section 5) has allowed speeding up algorithm processing times, which would be very large otherwise.

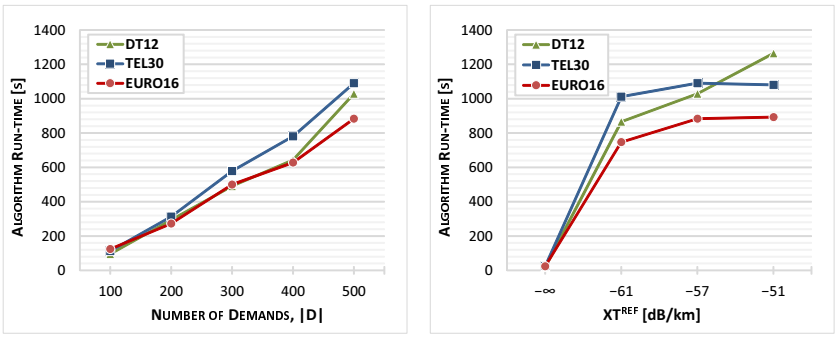

Figure 7. OSNR-LA-PSA computation times in a function of number of demands $|\mathcal{D}|$ for $XT^{\mathrm{REF}} = -57$ dB/km (left chart) and reference crosstalk level XT^{REF} for $|\mathcal{D}| = 500$ (right chart).

7. Conclusions

In this paper, we have addressed the problem of quality-of-transmission-aware planning of lightpath connections in spectrally–spatially flexible optical networks connected using weakly coupled multi-core fibers. For estimation of QoT, we made use of an OSNR-based estimator in which the crosstalk impairment occurring in MCFs is considered as a source of the OSNR degradation along with other physical-layer impairments. The application of the OSRN model allows obtaining reliable solutions, which may not be the

case for the methods proposed in prior works that are based on the verification of XT levels only. We have included the OSNR estimator into a mixed-integer programming model of the lightpath planning optimization problem as a set of problem variables and constraints. Moreover, in order to generate solutions for larger network instances, we have developed an effective and fast optimization method.

The obtained results of numerical experiments show that the MIP model has a low scalability, especially at the presence of crosstalk impairment, which complicates significantly solving the model. On the contrary, the optimization method proposed is capable of generating good quality solutions and can provide solutions to larger problem instances in reasonable time, even though the XT effect has a negative impact on algorithm computation times, too. Inter-core crosstalk also affects network performance and may lead to much higher demand for spectrum resources— even twice as much in the evaluated network scenarios—when compared to the case where this signal impairment is not present. Eventually, the capacity of a multi-core fiber may not be utilized fully it the MCF has a specific core arrangement that does not allow to utilize some of its cores due to excessive XT levels in these cores. In particular, we have shown that a six-core MCF that has a core arrangement corresponding to a typical seven-core MCF, but is deprived of the central core, may offer almost the same performance as the seven-core MCF in the networks in which crosstalk has a considerable impact on transmission quality.

In future works, we will focus on reformulating and strengthening the MIP model proposed in this work, with the aim of enabling solving larger problem instances as well as improving the estimation of solution lower bounds.

Author Contributions: Conceptualization, M.K.; Funding acquisition, M.K.; Investigation, M.K. and M.J.; Methodology, M.K. and M.J.; Project administration, M.K.; Software, M.K.; Supervision, M.K.; Visualization, M.K.; Writing—original draft, M.K.; Writing—review and editing, M.K. and M.J. All authors have read and agreed to the published version of the manuscript.

Funding: This research was funded by National Science Centre, Poland under grants number 2016/21/B/ST7/02212 and 2018/31/B/ST7/03456.

Institutional Review Board Statement: Not applicable.

Informed Consent Statement: Not applicable.

Data Availability Statement: Not applicable.

Conflicts of Interest: The author declares no conflict of interest.

Abbreviations

The following abbreviations are used in this manuscript:

EON	Elastic optical network
MCF	Multi-core fiber
MF	Modulation format
MIP	Mixed-integer programming
OC	Optical carrier
OSNR	Optical signal-to-noise ratio
OSNR-LA	OSNR-aware lightpath allocation
OSNR-LA-PSA	OSNR-aware lightpath allocation–parallel simulated annealing method
PLI	Physical-layer impairment
QoT	Quality of transmission
RSSA	Routing, spatial mode and spectrum allocation
SDM	Space division multiplexing
SNR	Signal-to-noise ratio
SCh	Super-channel
SS-FON	Spectrally and spatially flexible optical network
TR	Transmission reach
XT	Crosstalk

References

1. Agiwal, M.; Roy, A.; Saxena, N. Next Generation 5G Wireless Networks: A Comprehensive Survey. *IEEE Commun. Surv. Tutor.* **2016**, *18*, 1617–1655. [CrossRef]
2. Saridis, G.M.; Alexandropoulos, D.; Zervas, G.; Simeonidou, D. Survey and Evaluation of Space Division Multiplexing: From Technologies to Optical Networks. *IEEE Commun. Surv. Tutor.* **2015**, *17*, 2136–2156. [CrossRef]
3. Gerstel, O.; Jinno, M.; Lord, A.; Yoo, S.J.B. Elastic Optical Networking: A New Dawn for the Optical Layer? *IEEE Comm. Mag.* **2012**, *50*, 12–20. [CrossRef]
4. Agrell, E.; Karlsson, M.; Chraplyvy, A.; Richardson, D.; Krummrich, P.; Winzer, P.; Roberts, K.; Fischer, J.; Savory, S.; Eggleton, B.; et al. Roadmap of optical communications. *J. Opt.* **2016**, *18*, 1–40. [CrossRef]
5. Shariati, B.; Klonidis, D.; Tomkos, I.; Marom, D.; Blau, M.; Ben-Ezra, S.; Gerola, M.; Siracusa, D.; Macdonald, J.; Psaila, N.; et al. Realizing Spectrally-Spatially Flexible Optical Networks. *IEEE Photon Soc. Newsl.* **2017**, *31*, 4–9.
6. Awaji, Y.; Sakaguchi, J.; Puttnam, B.J.; Luis, R.S.; Mendinueta, J.M.D.; Klaus, W.; Wada, N. High-Capacity Transmission over Multi-Core Fibers. *Opt. Fiber Technol.* **2017**, *35*, 100–107. [CrossRef]
7. Goścień, R.; Walkowiak, K.; Klinkowski, M. Distance-Adaptive Transmission in Cloud-Ready Elastic Optical Networks. *IEEE/OSA J. Opt. Commun. Netw.* **2014**, *6*, 816–828. [CrossRef]
8. Klinkowski, M.; Lechowicz, P.; Walkowiak, K. Survey of Resource Allocation Schemes and Algorithms in Spectrally-Spatially Flexible Optical Networking. *Opt. Switch. Netw.* **2018**, *27*, 58–78. [CrossRef]
9. Hayashi, T.; Taru, T.; Shimakawa, O.; Sasaki, T.; Sasaoka, E. Design and Fabrication of Ultra-Low Crosstalk and Low-Loss Multi-Core Fiber. *Opt. Express* **2011**, *19*, 16576–16592. [CrossRef]
10. Shariati, B.; Mastropaolo, A.; Diamantopoulos, N.P.; Rivas-Moscoso, J.M.; Klonidis, D.; Tomkos, I. Physical-Layer-Aware Performance Evaluation of SDM Networks Based on SMF Bundles, MCFs, and FMFs. *IEEE/OSA J. Opt. Commun. Netw.* **2018**, *10*, 712–722. [CrossRef]
11. Tode, H.; Hirota, Y. Routing, Spectrum, and Core and/or Mode Assignment on Space-Division Multiplexing Optical Networks. *IEEE/OSA J. Opt. Commun. Netw.* **2017**, *9*, A99–A113. [CrossRef]
12. Yang, M.; Zhang, Y.; Wu, Q. Routing, Spectrum, and Core Assignment in SDM-EONs With MCF: Node-Arc ILP/MILP Methods and an Efficient XT-Aware Heuristic Algorithm. *IEEE/OSA J. Opt. Commun. Netw.* **2018**, *10*, 195–208. [CrossRef]
13. Perello, J.; Gene, J.M.; Pages, A.; Lazaro, J.A.; Spadaro, S. Flex-Grid/SDM Backbone Network Design with Inter-Core XT-Limited Transmission Reach. *IEEE/OSA J. Opt. Commun. Netw.* **2016**, *8*, 540–552. [CrossRef]
14. Klinkowski, M.; Zalewski, G. Dynamic Crosstalk-Aware Lightpath Provisioning in Spectrally-Spatially Flexible Optical Networks. *IEEE/OSA J. Opt. Commun. Netw.* **2019**, *11*, 213–225. [CrossRef]
15. Walkowiak, K.; Klinkowski, M.; Lechowicz, P.; Sen, A. ILP Modeling of Flexgrid SDM Optical Networks. In Proceedings of the 2016 17th International Telecommunications Network Strategy and Planning Symposium (Networks), Montreal, QC, Canada, 26–28 September 2016; pp. 1–3.
16. Rottondi, C.; Boffi, P.; Martelli, P.; Tornatore, M. Routing, Modulation Format, Baud Rate and Spectrum Allocation in Optical Metro Rings with Flexible Grid and Few-Mode Transmission. *IEEE J. Lightw. Technol.* **2017**, *1*, 61–70. [CrossRef]
17. Muhammad, A.; Zervas, G.; Simeonidou, D.; Forchheimer, R. Routing, Spectrum and Core Allocation in Flexgrid SDM Networks with Multi-core Fibers. In Proceedings of the 2014 International Conference on Optical Network Design and Modeling, Stockholm, Sweden, 19–22 May 2014; pp. 192–197.
18. Muhammad, A.; Zervas, G.; Forchheimer, R. Resource Allocation for Space Division Multiplexing: Optical White Box vs. Optical Black Box Networking. *IEEE J. Lightw. Technol.* **2015**, *33*, 4928–4941. [CrossRef]
19. Shariati, B.; Khodashenas, P.S.; Rivas-Moscoso, J.M.; Ben-Ezra, S.; Klonidis, D.; Jimenez, F.; Velasco, L.; Tomkos, I. Evaluation of the Impact of Different SDM Switching Strategies in a Network Planning Scenario. In Proceedings of the Optical Fiber Communication Conference, Anaheim, CA, USA, 20–24 March 2016; pp. 1–3.
20. Fujii, S.; Hirota, Y.; Tode, H.; Murakami, K. On-Demand Spectrum and Core Allocation for Multi-Core Fibers in Elastic Optical Network. In Proceedings of the Optical Fiber Communication Conference, Anaheim, CA, USA, 17–21 March 2013; pp. 1–3.
21. Tode, H.; Hirota, Y. Routing Spectrum and Core Assignment for Space Division Multiplexing Elastic Optical Networks. In Proceedings of the 2014 16th International Telecommunications Network Strategy and Planning Symposium (Networks), Funchal, Portugal, 17–19 September 2014; pp. 1–7.
22. Muhammad, A.; Zervas, G.; Saridis, G.; Salas, E.H.; Simeonidou, D.; Forchheimer, R. Flexible and Synthetic SDM networks with Multi-Core-Fibers Implemented by Programmable ROADMs. In Proceedings of the 2014 The European Conference on Optical Communication (ECOC), Cannes, France, 21–25 September 2014; pp. 1–3.
23. Perello, J.; Gene, J.M.; Lazaro, J.A.; Pages, A.; Spadaro, S. Assessment of Flex-Grid/SDM Backbone Networks under Inter-Core XT-limited Transmission Reach. In Proceedings of the 2015 International Conference on Photonics in Switching (PS), Florence, Italy, 22–25 September 2015; pp. 1–3.
24. Klinkowski, M.; Ksieniewicz, P.; Jaworski, M.; Zalewski, G.; Walkowiak, K. Machine Learning Assisted Optimization of Dynamic Crosstalk-Aware Spectrally-Spatially Flexible Optical Networks. *IEEE J. Lightw. Technol.* **2020**, *38*, 1625–1635. [CrossRef]
25. Li, Y.; Li, Y.; Hua, N.; Zheng, X. Shared Backup Path Protection in Multi-Core Fiber Networks with MIMO-based Crosstalk Suppression. In Proceedings of the Optical Fiber Communication Conference, Anaheim, CA, USA, 20–24 March 2016; pp. 1–3.

26. Yao, Q.; Yang, H.; Zhao, Y.; Zhu, R.; Zhang, J.; Wu, J. Crosstalk-aware Routing, Spectrum, and Core Assignment in Elastic Optical Networks with Multi-core Fibers. In Proceedings of the 2016 Asia Communications and Photonics Conference (ACP), Wuhan, China, 2–5 November 2016.
27. Marom, D.M.; Blau, M. Switching solutions for WDM-SDM optical networks. *IEEE Comm. Mag.* **2015**, *53*, 60–68. [CrossRef]
28. Poggiolini, P. The GN Model of Non-Linear Propagation in Uncompensated Coherent Optical Systems. *IEEE J. Lightw. Technol.* **2012**, *30*, 3857–3879. [CrossRef]
29. Poggiolini, P.; Bosco, G.; Carena, A.; Cigliutti, R.; Curri, V.; Forghieri, F.; Pastorelli, R.; Piciaccia, S. The LOGON Strategy for Low-Complexity Control Plane Implementation in New-Generation Flexible Networks. In Proceedings of the Optical Fiber Communication Conference, Anaheim, CA, USA, 17–21 March 2013.
30. Klinkowski, M.; Walkowiak, K. An Efficient Optimization Framework for Solving RSSA Problems in Spectrally and Spatially Flexible Optical Networks. *IEEE/ACM Trans. Netw.* **2019**, *27*, 1474–1486. [CrossRef]
31. Talbi, E.G. *Metaheuristics: From Design to Implementation*; Wiley: Hoboken, NJ, USA, 2009.
32. Elson, D.J.; Beppu, S.; Takahashi, H.; Tsuritani, T. Comparison of Intercore-Crosstalk Sources for Multicore Fibre in Recirculating Loop Transmission. In Proceedings of the 2020 Opto-Electronics and Communications Conference (OECC), Taipei, Taiwan, 4–8 October 2020.
33. Matsui, T.; Sagae, Y.; Sakamoto, T.; Nakajima, K. Design and Applicability of Multi-core Fibers with Standard Cladding Diameter. *IEEE J. Lightw. Technol.* **2020**, *38*, 6065–6070. [CrossRef]
34. Carena, A.; Curri, V.; Bosco, G.; Poggiolini, P.; Forghieri, F. Modeling of the Impact of Nonlinear Propagation Effects in Uncompensated Optical Coherent Transmission Links. *IEEE J. Lightw. Technol.* **2012**, *30*, 1524–1539. [CrossRef]
35. IBM. ILOG CPLEX Optimizer. 2022. Available online: http://www.ibm.com (accessed on 12 July 2022).